Performance comparison between Surface Mounted and Interior PM motor drives for Electric Vehicle application

Performance comparison between Surface Mounted and Interior PM motor drives for Electric Vehicle application

Gianmario Pellegrino, *Member, IEEE*, Alfredo Vagati, *Fellow, IEEE*,
Paolo Guglielmi, *Member, IEEE*, and Barbara Boazzo

***Abstract* – Electric Vehicles make use of permanent magnet synchronous traction motors for their high torque density and efficiency. A comparison between interior permanent magnet (IPM) and surface mounted permanent magnet (SPM) motors is carried out, in terms of performance at given inverter ratings. The results of the analysis, based on a simplified analytical model and confirmed by FE analysis, show that the two motors have similar rated power but that the SPM motor has barely no overload capability, independently of the available inverter current. Moreover the loss behavior of the two motors is rather different in the various operating ranges with the SPM one better at low speed due to short end connections but penalized at high speed by the need of a significant de-excitation current. The analysis is validated through finite-element simulation of two actual motor designs.**

***Index Terms*—Electric Vehicle, PM Synchronous motors, PM motor drives, Constant-power speed range, Iron loss, High speed AC drives.**

I. INTRODUCTION

The diffusion of Electric Vehicles (EV) in the urban context is only matter of time, since adoption of zero emission vehicles, either powered by chemical accumulators or fuel cells, is becoming mandatory, for the well known reasons. Indeed, this adoption will be gradual, also for the related need of infrastructures, but it is already accepted that EVs will represent the solution for urban mobility in the next future.

On the other hand, the choice of the electric drive-train most suited to this application is still matter of discussions. The most used electric motors in this sense are up to now induction motors (IM) and permanent magnet (PM) synchronous motors [1]. The former are adopted for their ruggedness and availability, while the latter are generally chosen for their higher torque density and efficiency.

Among PM motors, surface-mounted (SPM) and interior PM (IPM) types are both considered [1-2], and an exhaustive comparison between the respective performances has not been made yet. In [3] a thorough comparison is carried out for a starter-generator. Most of the more recent research in this field has being devoted to motors with non overlapping windings, either with SPMs [4-5] or IPMs [6-7], though such IPM machines are often very similar to SPM ones for magnets layout and for having rather a low saliency. Moreover, it is recognized that concentrated windings reduce the saliency of any IPM machine and thus part of their specific advantages that are related to the reluctance torque component [8]. For these reasons this paper focuses on the comparison between a SPM machine with concentrated windings and an IPM machine with distributed windings and four flux barriers per pole. As evidenced by Fig. 1, the selected machine types are at the opposite ends of the spectrum in terms of manufacturing complexity. Most of other combinations such as simpler IPM rotors and stators, including fractional slots ones, stay in between the two considered here.

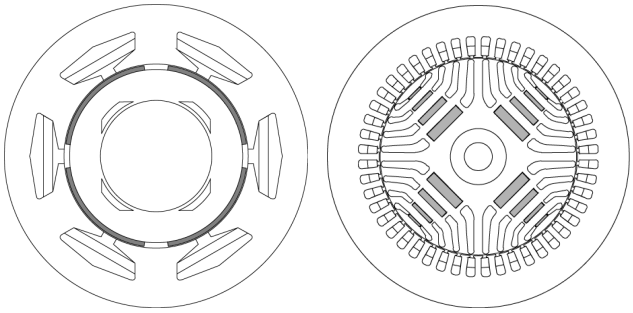

Figure 1. Example motors, having the same continuous torque, power and current (P_1, T_1, i_1). The two motors have the same stator diameter and stack length.

The paper follows the work presented in [9] where the SPM and IPM motor drives have been compared at given vehicle specification and inverter size. It was shown that:

- the continuous power of SPM and IPM motors is practically the same.
- The SPM motor is easier to manufacture, and has shorter end connections and then a bit shorter overall length.
- The IPM motor has a very good overload capability, over the entire speed range, while the SPM motor has not, independently of the applied current.
- High speed losses affect both the motors, due to PM losses for SPM and slot harmonic losses for IPM.

In this paper the results of [9] are reviewed and further aspects of the comparison are outlined:

- The efficiency maps over the whole torque versus speed operation area.
- The detail of the different losses of the two motors.
- The different behavior at partial load.

A. *Specifications of an EV drive*

In general, EVs require a constant-torque region at low speed and a constant-power region at high speed [10]. The continuous torque at low speed is dictated by the maximum slope specified for hill climbing, while the continuous power

Manuscript received December 20, 2010. Accepted for publication April 6, 2011.

G. Pellegrino, A. Vagati, P. Guglielmi and B. Boazzo are with the Department of Electrical Engineering, Politecnico di Torino, 10129 Torino, Italy (e-mail: gianmario.pellegrino@polito.it, alfredo.vagati@polito.it, paolo.guglielmi@polito.it, barbara.boazzo@polito.it)

determines the maximum cruising speed of the vehicle. Intermittent overload for short durations is required for vehicle accelerations at any speed. At overload, the motor is thermally safe at least for a couple of minutes while the inverter and battery maximum ratings limit the output power: i.e. the inverter current determines the maximum torque while in general it is the battery that limits the maximum power. ***The overload capability typical of the electric motors is a great advantage with respect to internal combustion engine (ICE) driven vehicles and must be conveniently exploited in EVs***.

The characteristics of a traction drive for EV are sketched in a general form in Fig. 2: both rated (continuous line) and overload (dashed line) curves show constant torque and constant power zones. Quite often the obtained overload performance does not match Fig. 2 up to maximum speed due to voltage limitation. Nevertheless, overload is welcome at large speed too, either for accelerating or possibly to regenerate power. The overload feature is the key point of the comparison in [9].

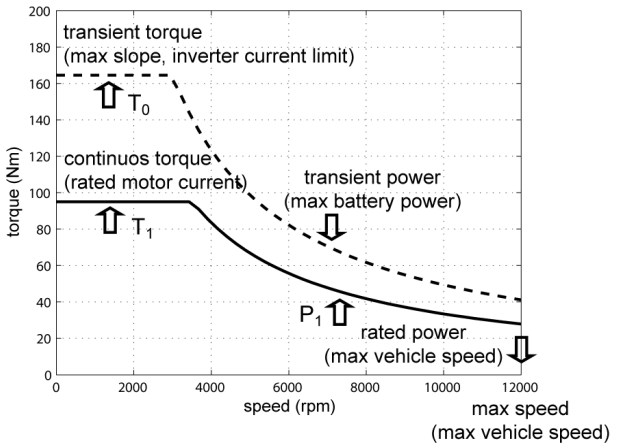

Figure 2. Example of schematic EV specification: rated (continuous) and overload (dashed) torque versus speed characteristics.

The power performance at base speed is not evidenced as one of the strict specifications in Fig.2 and it is normally introduced only as a reference point. In other words, once the basic performance requirements (T_1, T_0, P_1) are fulfilled, two drives can be comparable even if their power at base speed is not exactly the same.

Among the drive characteristics, efficiency has a particular importance, especially when the regenerative braking is exploited, like in urban cycle. For this type of workload a better efficiency of the motor drive can make the difference in terms of vehicle range. The efficiency comparison between two drives should refer to a specific vehicle cycle. As a general basis for comparison, efficiency maps over the entire torque – speed region will be given for the two motors, so that different driving cycles may be evaluated case by case.

Last, the quality of steel laminations plays a key role at high speed for both machines. For this reason the same high speed steel grade will be adopted for the two motors and the effects of this choice will be discussed.

II. MODELING OF THE SPM MOTOR DRIVE

A. *Power curve at continuous current i_1.*

In Fig. 3 the vector flux-weakening trajectories at rated current i_1 are shown for the SPM motor drive. In the constant-torque zone (point A_1) the current vector is in quadrature to the PM flux for maximum torque per Ampere (MTPA) operation. At higher speed the current vector is rotated to reduce the flux linkage and keep the voltage within the inverter limit. An ideal flat power curve is obtained if the current-dependent flux $L_{eq}\, i_1$ equals the PM flux linkage λ_m, [11] that is the situation shown in Fig. 3:

$$\lambda_m = L_{eq} \cdot i_1 \tag{1}$$

where L_{eq} is the SPM motor inductance. The corresponding power versus speed curve is reported in Fig. 4 (continuous line).

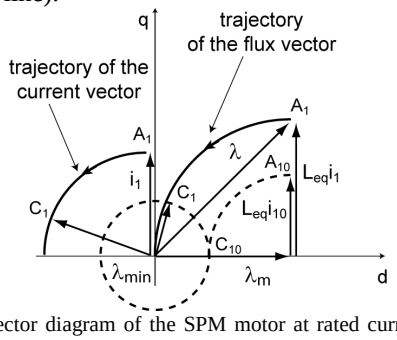

Figure 3. Vector diagram of the SPM motor at rated current (i_1) and at the no-load current amplitude needed at maximum speed (i_{10}).

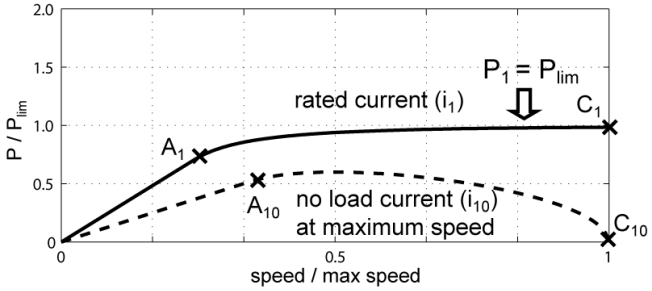

Figure 4. Per-unit power versus speed of the SPM motor at rated current (i_1) and no-load current, maximum speed (i_{10}).

At high speed, the power factor tends to one, since the flux and current vectors tend to be in quadrature to each other (Fig. 3, vectors in position C_1). Thus the power asymptotically tends to the limit value:

$$P_{lim} = \frac{3}{2} \cdot V \cdot i_1 \tag{2}$$

where V is the maximum phase voltage amplitude. In Fig. 4 the per-unit continuous power is plotted: if power losses are disregarded the output power curve has nearly the shape of the power factor. Therefore at base speed (point A_1) the p.u. power is nearly 0.7 (Fig. 4) as the power factor is (the current leads the flux vector by 45 degrees in Fig. 3).

In Fig. 3, λ_{min} is representative of the flux amplitude to be respected at maximum speed, to cope with the voltage limit:

$$\lambda_{\min} = \frac{V}{\omega_{\max}} \tag{3}$$

λ_{min} is given by (3), where the resistive drop has been disregarded. Because of the voltage limit, also at partial load and no-load the flux amplitude must be limited, at high speed, by means of a de-magnetizing current. In particular, the worst-case de-magnetizing current i_{10} is represented in Fig. 3 and its amplitude is:

$$i_{10} = i_1 \cdot \left(1 - \frac{\lambda_{min}}{\lambda_m}\right) \tag{4}$$

The need for some flux-weakening current at light and no-

load is a general drawback of this kind of motors, because it implies more copper losses. Most of the time the drive is at partial load in the speed range above the base speed. In such cases only a small part of the motor current is actually giving torque while ***the most of Joule losses are spent just for flux weakening***, as will be evidenced in section V.

As said $P_1 = P_{lim}$ is the continuous power, determined by the maximum vehicle speed specification. Thus, the motor rated current i_1 must match the power dissipation allowed by the motor cooling, while the PM flux λ_m must be maximized for obtaining an optimal torque to current ratio. As a consequence, the only parameter left to satisfy (1) is the motor inductance L_{eq}, which must be properly designed at that aim. This generally implies the adoption of a fractional number of slots per pole per phase, as it will be discussed in the following [5].

B. Power curve at overload current i_0.

In Fig. 5 the vector diagram at overload is shown, with reference to a current i_0 that is 173% of the continuous current i_1 (i.e. 3 times the Joule losses). At low speed, the power factor is quite low and the voltage limit is met very soon, because of the larger flux amplitude. From the constant torque working point (A_0 in Fig. 5) the current is rotated until the flux vector is aligned to the *q* axis (B_0 in Fig. 5), which represents the maximum torque per voltage (MTPV) flux condition [11]. To increase the speed further, the flux is kept along the *q* axis by reducing the i_q component only, with the i_d current equal to the characteristic current i_1 (1).

The MTPV flux amplitude (5) is proportional to the torque current component i_q:

$$\lambda_{MTPV} \equiv \lambda_q = L_{eq} \cdot i_{q,MTPV} \tag{5}$$

that is reduced proportionally to the speed (6) because of the constant voltage *V*.

$$i_{q,MTPV} = \frac{\lambda_{MTPV}}{L_{eq}} = \frac{V}{\omega L_{eq}} \tag{6}$$

As for the *q*-current, the torque also varies inversely with speed (7) and consequently the power results to be constant with speed (8), and equal to the P_{lim} value (2).

$$T_{MTPV} = \tfrac{3}{2}\, p \cdot \lambda_m \cdot i_{q,MTPV} = \tfrac{3}{2}\, p \cdot \frac{\lambda_m}{L_{eq}} \cdot \frac{V}{\omega} \tag{7}$$

$$P_{MTPV} = \tfrac{3}{2} \cdot \frac{\lambda_m}{L_{eq}} \cdot V = \tfrac{3}{2} \cdot V \cdot i_1 = P_{lim} \tag{8}$$

The condition (1) has been substituted in (8).

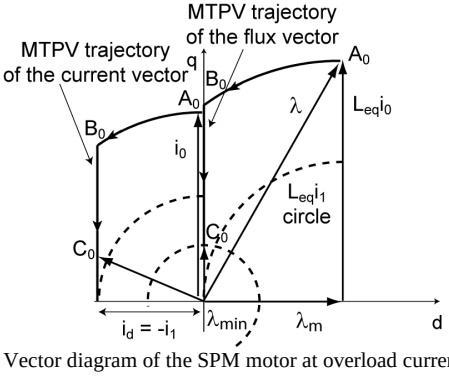

Figure 5. Vector diagram of the SPM motor at overload current i_0.

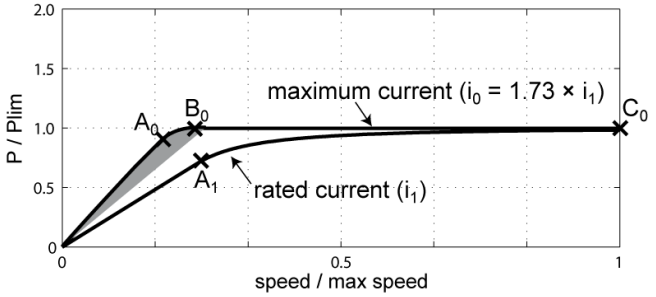

Figure 6. Per-unit power versus speed of the SPM motor at rated current (i_1) and 173% overload current (i_0).

Once the MTPV limit is reached the output power is clamped to P_{lim} according to (8), independently of the available current overload. In other words, the 173% overload current i_0 produces an overload torque below the base speed, as represented in Fig. 6, but the power overload vanishes as the speed increases beyond that point.

III. IPM MOTOR DRIVE

A. Power curve at rated current i_1

The torque of the IPM motor show both PM flux and anisotropy terms:

$$T = \tfrac{3}{2}\, p \cdot \left[\lambda_m \cdot i_q - L_d (\xi - 1) \cdot i_d \cdot i_q \right] \tag{9}$$

where $\xi = L_q / L_d$ is the saliency ratio. For MTPA operation i_d is negative (Fig. 7) with an MTPA phase angle that varies from motor to motor. For flux weakening the current vector is rotated from the MTPA angle towards the MTPV locus, if any. As for the SPM, when the relationship (10) is true, the flux vector at rated current is driven towards zero and the MTPV locus is not met (Fig. 7), while it is met at overload current.

$$\lambda_m = \frac{L_q}{\xi} \cdot i_1 \tag{10}$$

Since L_q mainly depends on the airgap length, the λ_m value that fulfills (10) depends on the rotor anisotropy: the larger the anisotropy is, the lower λ_m is. In the SPM case there is a unique inductance value that depends on the stator design (type of winding, internal diameter, slot shape) and the magnet thickness, while here the *d*-axis inductance can be varied by means of ξ that relies basically on the rotor design. If ξ is maximized, then the PM flux needed to match (10) can be reduced with no loss of torque due to the increase of the reluctance torque in (9). The vector diagrams of two IPM motors designed according to (10), with same flux and current but different saliencies are schematically represented in Fig. 7. The λ_r flux (where *r* stands for *reluctance*) is the one produced by the stator current.

As shown in the following, both the IPM machines can have the same rated torque of the SPM machine of same size. At high speed, as the vectors go through the respective flux weakening trajectories dashed in Fig. 7, the angle between the current and flux vectors always tends to 90°, as it was for the SPM motor in Fig. 3. Moreover, if the SPM and IPM machines are designed for satisfying (1) and (10) respectively, and have the same rated flux and current, they reach the same high speed asymptotic power [11].

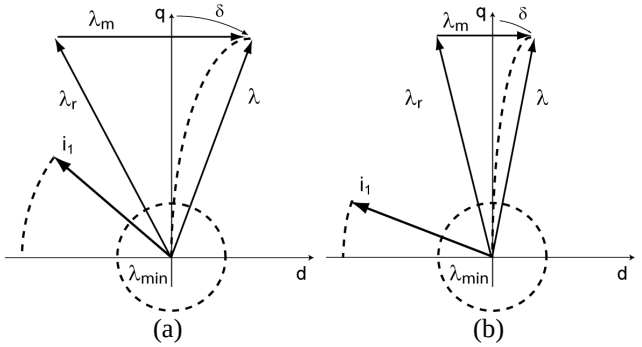

Figure 7. Vector diagrams of two IPM motors at rated current (i_1), in the respective MTPA conditions. The dashed curves are the trajectories of the flux and current vectors in flux weakening. a) motor with low anisotropy. b) motor with high anisotropy.

The power curve of the two IPM motors at rated current is reported in Fig. 10 (dashed) and it is identical to the one reported in Figs. 4 and 6 for the SPM motor. For all Figs. 4, 6 and 10 P_{lim} is the same. On the other hand, the low saliency IPM machine (Fig. 7a) has a λ_m flux that is comparable, in per-unit of the rated flux, to the one of the SPM machine. Also the related side effects are then comparable, namely the overvoltage in case of uncontrolled generator operation [12]. Instead, the high anisotropy motor (Fig. 7b) has much lower per-unit PM flux and side effects. In addition, the ***design with high-saliency and low λ_m improves the overload capability at large speed***, as shown in the following.

B. Overload current i_0 and possible design choices

The same current overload ratio $i_0 = 1.73\ i_1$ is considered for the IPM motor drive. The MTPV power is no longer clamped to an upper limit value (8), as it was for the SPM motor: nevertheless, the power curve in the MTPV region tend to drop with speed. For possibly having a flat power curve at overload it is convenient to design the IPM machine such that the MTPV zone is ***encountered exactly at the maximum speed, at overload current***, as it was proposed in [13]. Under such assumption, the flux vector diagram at maximum speed, overload current conditions is the one in Fig. 8. The equation describing the MTPV trajectory is:

$$sin\,\delta = \tfrac{1}{4}\cdot\left(-\alpha+\sqrt{\alpha^2+8}\right)\ ;\ \alpha = \frac{\lambda_m}{\lambda}\cdot\frac{\xi}{\xi-1} \quad (11)$$

where δ is the flux phase angle defined in Fig. 7. In Fig. 8 δ_{max} is the flux angle at overload, maximum speed ($\lambda = \lambda_{min}$ in eq. 11).

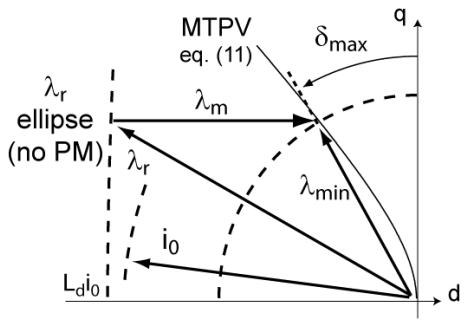

Figure 8. IPM motor flux diagram at maximum speed and overload current i_0: the MTPV locus is supposed to be met exactly at maximum speed, maximum current..

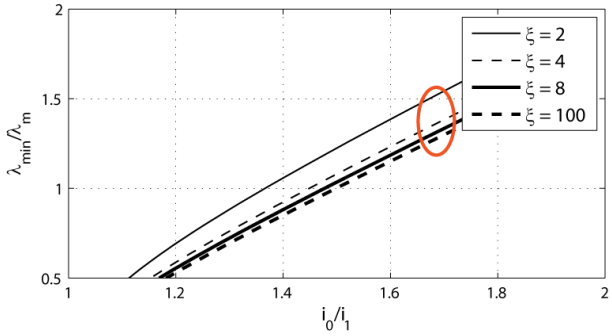

Figure 9. Minimum flux as a function of current overload and anisotropy ratio.

Equation (12) is obtained by inspection of the figure:

$$\frac{L_d\, i_0}{\lambda_{min}} \cong sin\,\delta_{max} + \frac{\lambda_m}{\lambda_{min}} \quad (12)$$

Substituting (10) in (12) the relationship (13) is obtained:

$$\frac{\lambda_{min}}{\lambda_m} = \left(sin\,\delta_{max}\right)^{-1}\cdot\left(\frac{i_0}{i_1}-1\right) \quad (13)$$

According to (13) the minimum flux increases with the current overload. As a consequence, from (3) and (13), ***the maximum speed that is feasible without encountering the MTPV reduces with the overload current***. The implicit equation (13) (δ_{max} depends of the flux ratio according to eq. 11) has been plotted in fig. 9 for better clarity. Given the overload ratio i_0/i_1 the ratio λ_{min}/λ_m follows, with little dependency on the motor saliency.

However, with a higher saliency λ_m is lower (and so it is λ_{min}) and the feasible maximum speed increases accordingly. To point out this, in Fig. 10 two IPM machines are compared: one with high saliency (ξ=8) and low PM flux (IPM1), and the other with low saliency (ξ=2), higher PM flux (IPM2).

The two machines are designed to give the same continuous power curve (P_1) with the same current (i_1) and voltage (V). IPM1 is designed to meet the MTPV at maximum speed, as explained, while IPM2 encounters the MTPV around 0.3 p.u. speed. Two conclusions can be drawn by inspection of Fig. 10:

- ***both IPM motors can be overloaded at low and high speed***, differently from the SPM case;
- ***the overload capability is much higher in those motors with a higher saliency.***

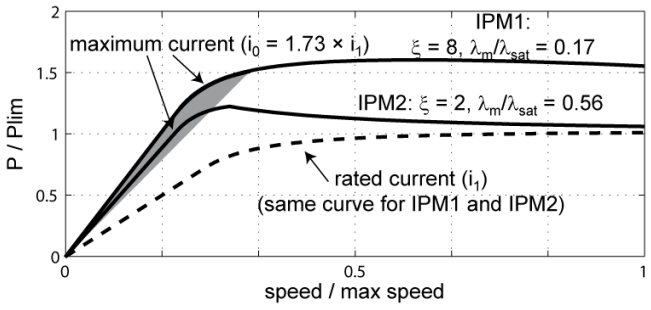

Figure 10. Per-unit power versus speed for two IPM motor drives with different saliency ratio and PM magnet flux, designed for the same continuous torque and power (T1 , P1) according to (10), and with the same rated flux (λ_{sat}).

C. Limitations of the adopted linear model

The curves of Figs. 4, 6, 10 (and also Fig. 11) have been obtained by means of linear machine models, for simplicity.

The performance at rated current is correctly represented by the model, because it is assumed that the rated flux amplitude (MTPA flux at rated current i_1) coincides with the core saturation limit (λ_{sat}) for all the considered motors. However, at overload the effects of saturation are not represented by the simplified model, that tend to overestimate the overload capability of all the considered machines (included the SPM one). For this reason a shaded area has been adopted in Figs. 6, 10 and 12 around the low speed overload zone, as a reminder of the limitations of this simplified model. Nevertheless, the simplified model is well representative of the behavior of the various machines in the flux weakened region, where saturation effects are less evident. As a validation, FEA calculated power curves are reported and discussed in section IV (Fig. 12).

D. Effect of reinforcing the PM flux.

The overload capability of IPM motors at high speed can be further improved if the PM flux is designed according to (14), that means higher than what considered so far according to (10).

$$\lambda_m = \frac{L_q}{\xi} \cdot \frac{i_1 + i_0}{2} \tag{14}$$

For a 173% overload the PM flux is increased by 36%. As a consequence, (13) becomes (15).

$$\frac{\lambda_{min}}{\lambda_m} = (sin\,\delta_{max})^{-1} \cdot \left(\frac{i_0}{i_1} - 1\right) \cdot \left(\frac{i_0}{i_1} + 1\right)^{-1} \tag{15}$$

The minimum flux ratio (15) is roughly reduced by 2.73 times with respect to (13), and the maximum speed that is feasible with no MTPV limitation is two times higher (2.73 / 1.36).

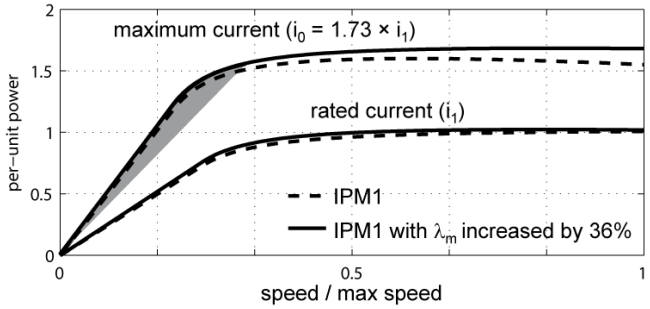

Figure 11. Effect of increased PM flux on overload capability: per-unit power vs speed curves for IPM1 (same as Fig. 8) and IPM1 with PM flux increased by 36% according to (13).

In Fig. 11 the power vs speed curves are shown for the high anisotropy machine IPM1 (ξ = 8) both at rated and at overload with the PM designed according to (10) and (13) respectively. Dotted lines are the IPM1 curves of Fig. 10. As said, the rated performance has no practical modification, while the overload performance is improved. Fig. 11 also shows that ***the design of PM flux is not critical for high saliency motors***. Again, the comparison of Fig. 11 with Fig. 6 points out the dramatic difference between SPM and IPM motors, as concerns the overload capability.

IV. Design and Comparison of Two Example Motors

Up to this point the motor design was not considered at all, except for the assumptions made with (1) and (10). An exhaustive comparison necessarily deals with actual design restrictions, i.e. thermal limits given by losses and the torque density and efficiency that can be obtained according to. To this aim, two example designs are reported in the following, with the common assumptions of:

- outer diameter (216 mm) and stack length (170 mm);
- 50kW continuous power at 12000 rpm maximum speed;
- 173% current overload.

Both the machines are liquid cooled. The phase rated voltage is 173V pk. Due to the impact of iron loss at large speed values, a good quality steel (M250-35A) has been used, for both designs. The same PM grade is also adopted (BMN-38SH).

With such design specifications, it turned out that the rated current for both machines is 208 A (pk) and the overload current is 360 A (pk). The SPM motor has shorter end-connections (8% of active length against 17%) and a larger copper cross section (+ 33%) resulting in a phase resistance of 21 mΩ (SPM) versus 26 mΩ (IPM) at 130 ° C. The numbers of turns in series per phase are 23 and 20 respectively. If the total slot cross section of the IPM motor was made the same of the one of the SPM, the motor would have still had the same continuous power with less Joule losses, but the overload capability would have been partially limited. It is worth to notice that the PM quantity of the IPM rotor is 40% higher than the one of the SPM rotor. This is not a general rule and depends on the two specific designs. The actual IPM motor was not optimized, from this point of view. With different design choices the PM quantity comparison could have given different results. Still, ***it remains true that choosing an IPM motor instead of a SPM one is not a matter of reducing the cost of the permanent magnets***, as could have been expected.

The evaluation of the rated and overload power curves and a thorough comparison of power losses and efficiency will be given in the following.

TABLE I – RATINGS OF THE TWO MOTOR DESIGNS.

		SPM	IPM
Pole pairs		2	2
Stator slots		48	6
Number of turns		23	20
Stator outer diameter	mm	216	
Stator inner diameter	mm	131	142
Stack length	mm	170	
Airgap	mm	0.7	
Base speed	rpm	3500	3500
Max speed	rpm	12000	
Continuous torque	Nm	110	110
Continuous current	A pk	208	208
Overload torque	Nm	135	200
Overload current	A pk	360	360
Characteristic current (PMs at 20°C)	A pk	226	230
Phase rated voltage	V pk	173	173
Phase back-emf (12000 rpm, PMs at 20°C)	V pk	554	152
Phase resistance at 130°C	Ω	0.021	0.026
Steel grade		M250–35A	
PM grade		BMN-38SH	
PM quantity	kg	1.35	1.95

A. *SPM motor design*

The key point of the design is to satisfy the relationship (1), that is to match the short circuit current with the thermal and demagnetization current limits. To this aim, fractional slots are used, giving the additional benefit of shorter end connections [5]. Due to the high maximum speed, the pole number must be maintained as low as possible, for limiting the iron losses. As a consequence a 6 slots, 4 poles (1/2 slots/pole-phase) was chosen, with a double layer winding (Fig. 1, left). Another tentative solution was also tested, with 12 slots and 10 poles (2/5 slots/pole-phase) and abandoned due to excessive core and PM loss (the fundamental frequency was up to 1 kHz). It is supposed that the PMs are constrained into a non conductive retaining sleeve, such as a carbon fiber sleeve, for avoiding the additional eddy current losses related to some kind of conductive retention devices. However, the additional depth required for that sleeve has not been considered, in the magnetic design.

B. *IPM motor design*

With the aim of minimizing the *d*-axis inductance, a multiple barrier rotor structure was chosen, shown in Fig. 1 (right). Moreover, to reduce torque ripple and high speed losses the combination 24/20 of stator and rotor slots per pole pair was conveniently chosen [14]. The PM flux was designed according to (10). The mechanical robustness of the rotor at high speed is related to the proper design of the inter-layer iron ribs, in terms of placement and thickness. The rotor has been verified against maximum centrifugal stress with reference to a maximum speed of 14000 rpm that is 20% higher than the maximum operating speed.

C. *Power curves*

As shown in Fig.12, the two motors give the same continuous power curve, when supplied with the same current, at the same inverter voltage. The comparison of Fig. 12 with the curves based on the linear model of Figs. 6, 10 points out the effects of core saturation. The rated power curves are slightly affected by saturation, for both the motors. Though, the torque curves at overload are much different from the ones forecasted by the linear model, also at low speed. This is due to saturation and cross saturation effects. This one is clearly heavier in the SPM case, which gives a definitely lower overload torque, also at low speed.

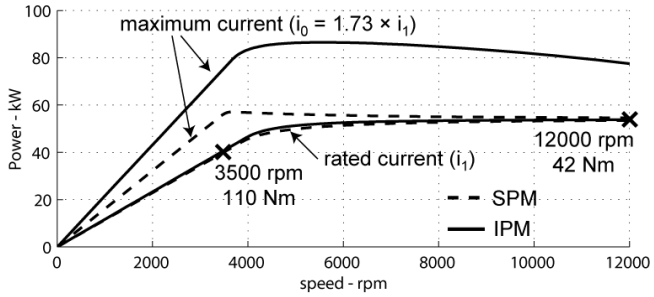

Figure 12. Example motors, having the same continuous torque, power and current (P_1, T_1, i_1). The two motors have the same stator diameter and stack length.

D. *FEA evaluation of the iron losses*

The core losses have been calculated by means of transient finite element analysis (FEA) over the whole torque and speed ranges of the two motors using MagNet, Infolytica. The iron loss model is based on the Epstein Frame loss measurements declared by the manufacturer and uses a modified Steinmetz equation augmented with an eddy current term to fit the loss manufacturer data. The accuracy of the model relies on the availability of loss curve data from the manufacturer at several frequencies, in particular at high frequency [15], and the M250-35A grade is characterized up to 2500 Hz.

E. *Loss and efficiency maps*

The loss maps of the two motors are reported in Figs. 13-14. The torque profile lined in white is the torque at rated current i_1 that is common to both motors, while the upper profiles of the maps are determined by the overload current i_0 and the overload area of the IPM motor is larger as said. The PM temperature is 100 °C. The PMs of the surface mounted machine are segmented tangentially in 5 parts, for reducing the eddy current losses and not segmented axially. The effect of axial segmentation will be discussed later.

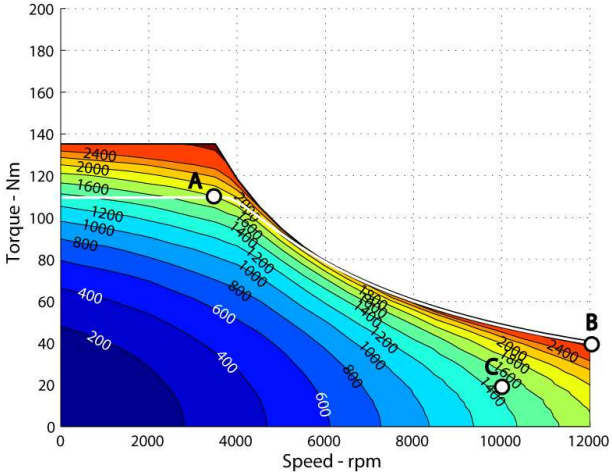

Figure 13. Total loss map of the SPM motor. The white line refer to the continuous current i_1 = 208 A (pk), the outside limit of the map refer to the overload current i_0 = 360 A (pk). PMs at 100° C. Copper at 130° C.

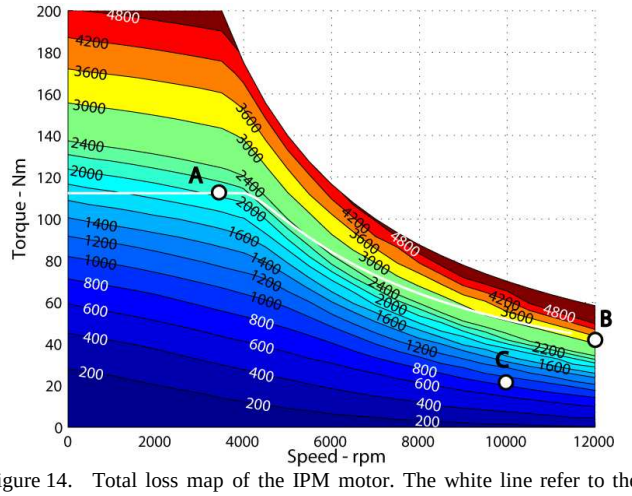

Figure 14. Total loss map of the IPM motor. The white line refer to the continuous current i_1 = 208 A (pk), the outside limit of the map refer to the overload current i_0 = 360 A (pk). PMs at 100° C. Copper at 130° C.

The two maps of Figs. 13-14 put in evidence that the losses of the IPM motor are progressive with the load torque at all speeds while the losses of the SPM motor are not, except for very low speed. As soon as the speed increases the SPM suffers from two terms of losses that are independent of the torque: PM losses and Joule losses due to the de-excitation current component (negative i_d), and this explains

the curled shape of the constant-loss curves in Fig. 13. On the other end, the IPM motor has little more copper losses and then higher loss overall at rated current due to the higher phase resistance. The harmonic losses of the IPM at high speed have been minimized by the specific 24-20 slot design [14]: with less rotor layers and less stator slots per pole higher core losses could be expected.

The efficiency maps are reported in Figs.15-16 showing that both the machines are rather efficient on the entire area of operation: as for the losses, the SPM motor is more efficient at low speed and much less at high speed.

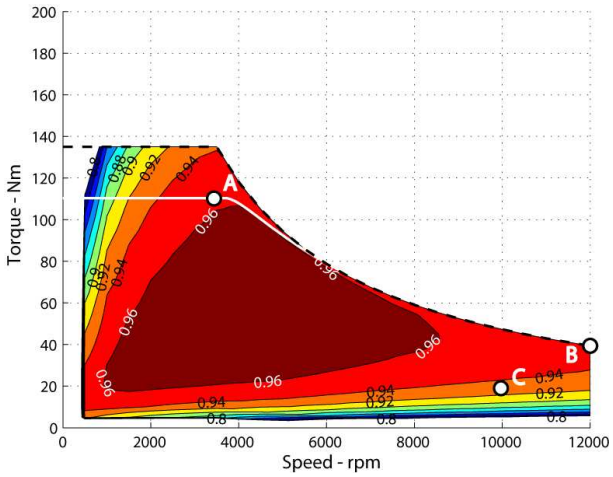

Figure 15. Efficiency map of the SPM motor. Same conditions as Fig. 13.

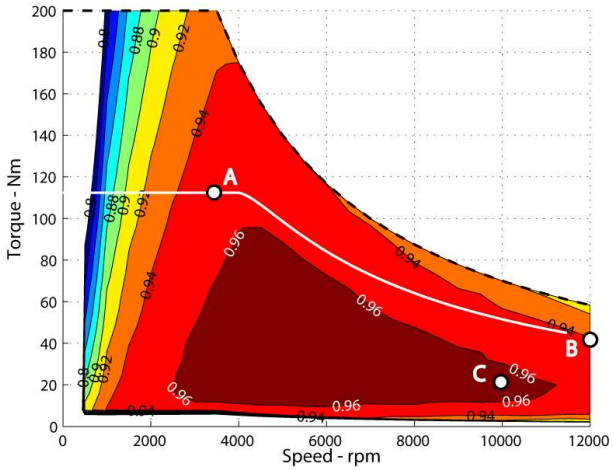

Figure 16. Efficiency map of the IPM motor. Same conditions as Fig. 14.

F. Detail of losses in specific points

Loss components are detailed for the three working points A, B and C put in evidence in Figs. 13-16:

- Point A (110 Nm, 3500 rpm) is representative of mild accelerations and decelerations in urban cycles.
- Point B (40 Nm, 12000 rpm) is cruising power at maximum speed.
- Point C (20 Nm, 10000 rpm) is cruising power at 80% of the maximum speed.

At the relatively low speed point A the losses have a dominant Joule term and a similar core terms. The losses are mainly on the stator and the IPM motor is less efficient in this area. At maximum speed, continuous power (point B) the SPM has significant PM losses that can be limited by further segmentation the PMs also in the axial direction [16]. Two options of axial segmentation are reported in the middle subfigure of Fig. 17. They show that for obtaining a significant reduction of the losses a troublesome 10-part segmentation would be required, added to the already assumed 5-part tangential segmentation.

Losses at point C show that the SPM Joule term is much higher despite the 20% lower resistance, due to the need of de-excitation current.

In case the operating speed specification was lower the SPM drive might have been helped by the possible adoption of a higher number of poles. If 10 or 14 poles are feasible, the continuous power density of the SPM motor can be higher [3], but still the IPM motor would maintain a much higher overload capability. Nevertheless, the actual trend in traction is to increase the speed as much as possible for reducing the motor size, and this makes high pole numbers unfeasible.

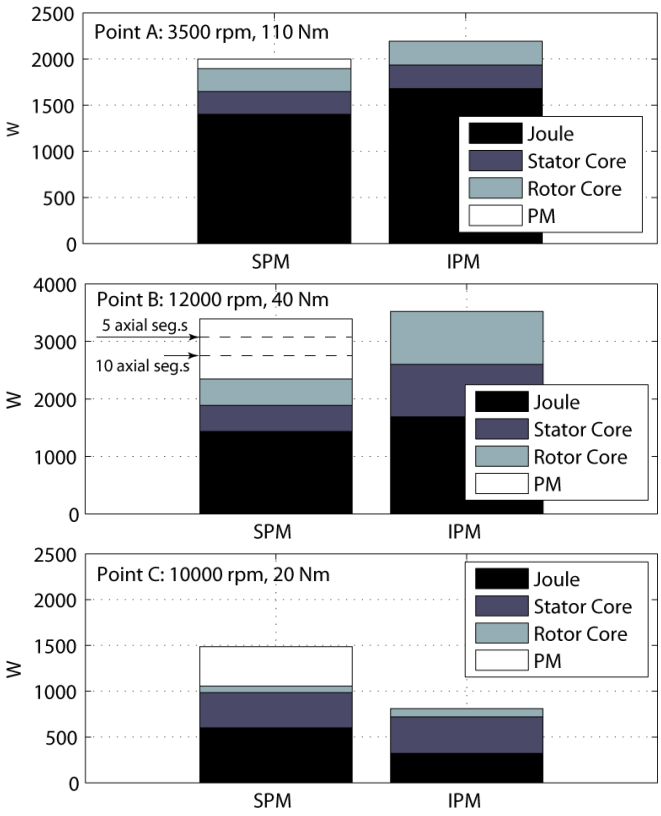

Figure 17. Detail of motor losses in the three working points A, B, C circled in Figs. 13-16.

V. Conclusions

Surface-mounted and interior-mounted PM synchronous motors have been thoroughly compared, for application to electric traction. The SPM motor has concentrated windings and a simpler construction. With equal active parts size and cooling ***the two motors give the same continuous power***. The IPM motor has a good overload capability over the entire speed range, if the saliency of the machine is maximized, while ***the output power of the SPM motor cannot overcome the continuous power rating independently of the applied current overload***. Dealing with losses and efficiency, the SPM motor is affected by ***extra-Joule losses for de-exciting the PM flux*** at high speed and PM losses that require segmentation in both directions (circumferential and axial). On the contrary, the IPM motor has higher Joule losses at low speed due to end connections and requires a properly ***high number of stator slots and***

rotor segments to keep the harmonic losses under control, that can make the fabrication more expensive.

VI. REFERENCES

[1] Zhu, Z.Q.; Chan, C.C.; "Electrical machine topologies and technologies for electric, hybrid, and fuel cell vehicles," *Vehicle Power and Propulsion Conference, 2008. VPPC '08. IEEE* , vol., no., pp.1-6, 3-5 Sept. 2008

[2] Chau, K.T.; Chan, C.C.; Chunhua Liu; , "Overview of Permanent-Magnet Brushless Drives for Electric and Hybrid Electric Vehicles," *Industrial Electronics, IEEE Transactions on* , vol.55, no.6, pp.2246-2257, June 2008

[3] El-Refaie, A.M.; Jahns, T.M., "Comparison of synchronous PM machine types for wide constant-power speed range operation," *Industry Applications Conference, 2005. Fourtieth IAS Annual Meeting. Conference Record of the 2005* , vol.2, no., pp. 1015-1022 Vol. 2, 2-6 Oct. 2005.

[4] EL-Refaie, A.M.; "Fractional-Slot Concentrated-Windings Synchronous Permanent Magnet Machines: Opportunities and Challenges," *Industrial Electronics, IEEE Transactions on* , vol.57, no.1, pp.107-121, Jan. 2010

[5] EL-Refaie, A.M.; Jahns, T.M., "Optimal flux weakening in surface PM machines using fractional-slot concentrated windings," *Industry Applications, IEEE Transactions on* , vol.41, no.3, pp. 790-800, May-June 2005

[6] Germishuizen, J.J.; Kamper, M.J.; , "IPM Traction Machine With Single Layer Non-Overlapping Concentrated Windings," *Industry Applications, IEEE Transactions on* , vol.45, no.4, pp.1387-1394, July-aug. 2009

[7] Chong, L.; Rahman, M.F.; , "Saliency ratio derivation and optimisation for an interior permanent magnet machine with concentrated windings using finite-element analysis," *Electric Power Applications, IET* , vol.4, no.4, pp.249-258, April 2010

[8] Soon-O Kwon; Sung-Il Kim; Peng Zhang; Jung-Pyo Hong; , "Performance comparison of IPMSM with distributed and concentrated windings," *Industry Applications Conference, 2006. 41st IAS Annual Meeting. Conference Record of the 2006 IEEE* , vol.4, no., pp.1984-1988, 8-12 Oct. 2006

[9] Vagati, A.; Pellegrino, G.; Guglielmi, P.; "Comparison between SPM and IPM motor drives for EV application," *Electrical Machines (ICEM), 2010 XIX International Conference on* , vol., no., pp.1-6, 6-8 Sept. 2010

[10] Ehsani, M.; Rahman, K.M.; Toliyat, H.A.; "Propulsion system design of electric and hybrid vehicles," *Industrial Electronics, IEEE Transactions on* , vol.44, no.1, pp.19-27, Feb 1997

[11] W. Soong and T. J. E. Miller, "Field weakening performance of brushless synchronous AC motor drives," Proc. IEE—Elect. Power Appl., vol. 141, no. 6, pp. 331–340, Nov. 1994.

[12] Jahns, T.M.; Caliskan, V.; , "Uncontrolled generator operation of interior PM synchronous machines following high-speed inverter shutdown," *Industry Applications, IEEE Transactions on* , vol.35, no.6, pp.1347-1357, Nov/Dec 1999

[13] P. Guglielmi, E. Armando, G. Pellegrino, A.Vagati, "Optimal design of IPM-PMASR motors for wide constant power speed range," Proc. of PCIM 2007, PCIM Europe, Nurnberg 2007- Germany.

[14] Pellegrino, G.; Guglielmi, P.; Vagati, A.; Villata, F.; , "Core loss and torque ripple in IPM machines: dedicated modeling and design trade off," *Energy Conversion Congress and Exposition, 2009. ECCE 2009. IEEE* , vol., no., pp.1911-1918, 20-24 Sept. 2009.

[15] Yamazaki, K.; Fukushima, N.; , "Experimental validation of iron loss model for rotating machines based on direct eddy current analysis of electrical steel sheets," *Electric Machines and Drives Conference, 2009. IEMDC '09. IEEE International* , vol., no., pp.851-857, 3-6 May 2009.

[16] J. L. Kirtley Jr., M. Tolikas, J. H. Lang, C.W. Ng, and R. Roche, "Rotor loss models for high speed PM motor-generators," in *Proc. ICEM'98*, 1998, pp. 1832–1837.

Gianmario Pellegrino (M'06) received the M.Sc. and Ph.D. degrees in electrical engineering from Politecnico di Torino, Turin, Italy, in 1998 and 2002, respectively.

He has been a Guest Researcher at Aalborg University, Denmark, in 2002. Since 2002 he has been with Politecnico di Torino, first as a Research Associate and then as an Assistant Professor, since 2007. He has been a visiting fellow at Nottingham University, UK, in 2010/2011. He is involved in research projects within the industry. He has more than 50 technical papers and one patent. His research areas are the electrical machines and drives, namely, the motor design and the digital control.

Dr. Pellegrino is an Associate Editor for the IEEE Transactions on Industry Applications. He is the corecipient of the IEEE-IAS EMC 3rd Paper Paper Award for ECCE 2009, the IEEE-IAS IDC 3rd Paper Paper Award for ECCE 2010 and the ICEM 2010 Best Paper Award.

Alfredo Vagati (M'88–SM'92–F'98) received the Laurea degree in Electrical Engineering from Politecnico di Torino, Turin, Italy, in 1970.

After a few years working in industry with Olivetti, he joined Politecnico di Torino in 1975, as Assistant Professor. In 1990, he became Professor of Electrical Machines and Drives at the University of Cagliari, Italy. In 1991, he rejoined Politecnico di Torino in the same capacity. From 1995 to 2003 He was the Head of the Electrical Engineering Department of Politecnico di Torino and member of the Academic Senate from 2005 to 2009. His scientific activity, in the field of electrical machines and drives, has been focused on high-performance ac drives. He has been involved in several industrial projects in the field of ac drives, as both a designer and a scientific reference. His most relevant activity has concerned the design and control of a family of newly developed, high-performance synchronous reluctance (SyR) an permanent magnet assisted synchronous reluctance (PMASR) motors. He has led several national and European research projects in the field of design and control of synchronous-machine-based drives for many different applications, including home appliances and the automotive world. He has authored or coauthored more than 100 technical papers.

Prof. Vagati is a Fellow Member of the IEEE Society. He is also a member of the Advisory Board of PCIM, International Conference and Exhibition.

Paolo Guglielmi (M'07) received the M.Sc. degree in electronic engineering and the Ph.D. degree in electrical engineering from the Politecnico di Torino, Turin, Italy, in 1996 and 2001, respectively.

In 1997, he joined the Department of Electrical Engineering, Politecnico di Torino, where he became an Assistant Professor in 2002. He has authored several papers published in technical journals and conference proceedings. His fields of interest include power electronics, high performance drives, and computer-aided design of electrical machines.

Barbara Boazzo received the M.Sc. degree in electrical engineering from Politecnico di Torino in 2010. She is currently a PhD student at the same university, working in the field of electric motors and drives.